Auxin carriers localization drives auxin accumulation in plant cells infected by Frankia in Casuarina glauca actinorhizal nodules.

Francine Perrine-Walker, Patrick Doumas, Mikael Lucas, Virginie Vaissayre, Nicholas J Beauchemin, Leah R Band, Jérome Chopard, Amandine Crabos, Geneviève Conejero, Benjamin Péret, et al.

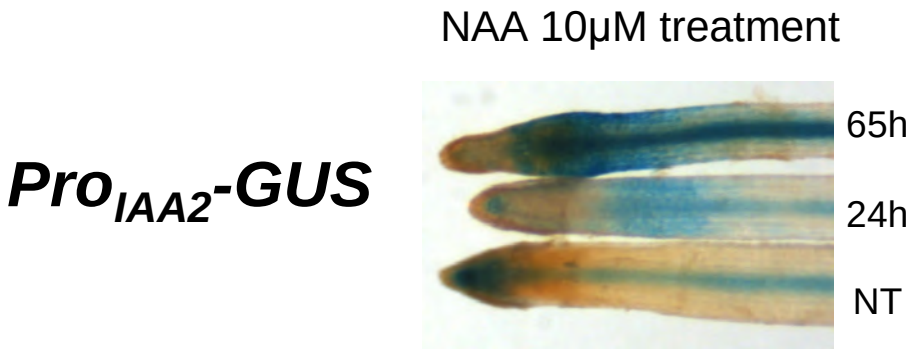

Fig. S1. Expression pattern of the *Pro$_{IAA2}$-GUS* molecular markers for auxin perception in *C. glauca*. Three markers were tested: *Pro$_{GH3}$-GUS*, *Pro$_{DR5}$-GUS* and *Pro$_{IAA2}$-GUS*. For these three markers similar results were observed. A weak expression was found in some transgenic plants in the vascular tissues and root meristems. Upon auxin treatment the markers were not or very weakly induced. Pictures of the root of transgenic *Pro$_{IAA2}$-GUS* plants treated with 10 µM NAA for 24h or 65h and a corresponding non-treated (NT) root.

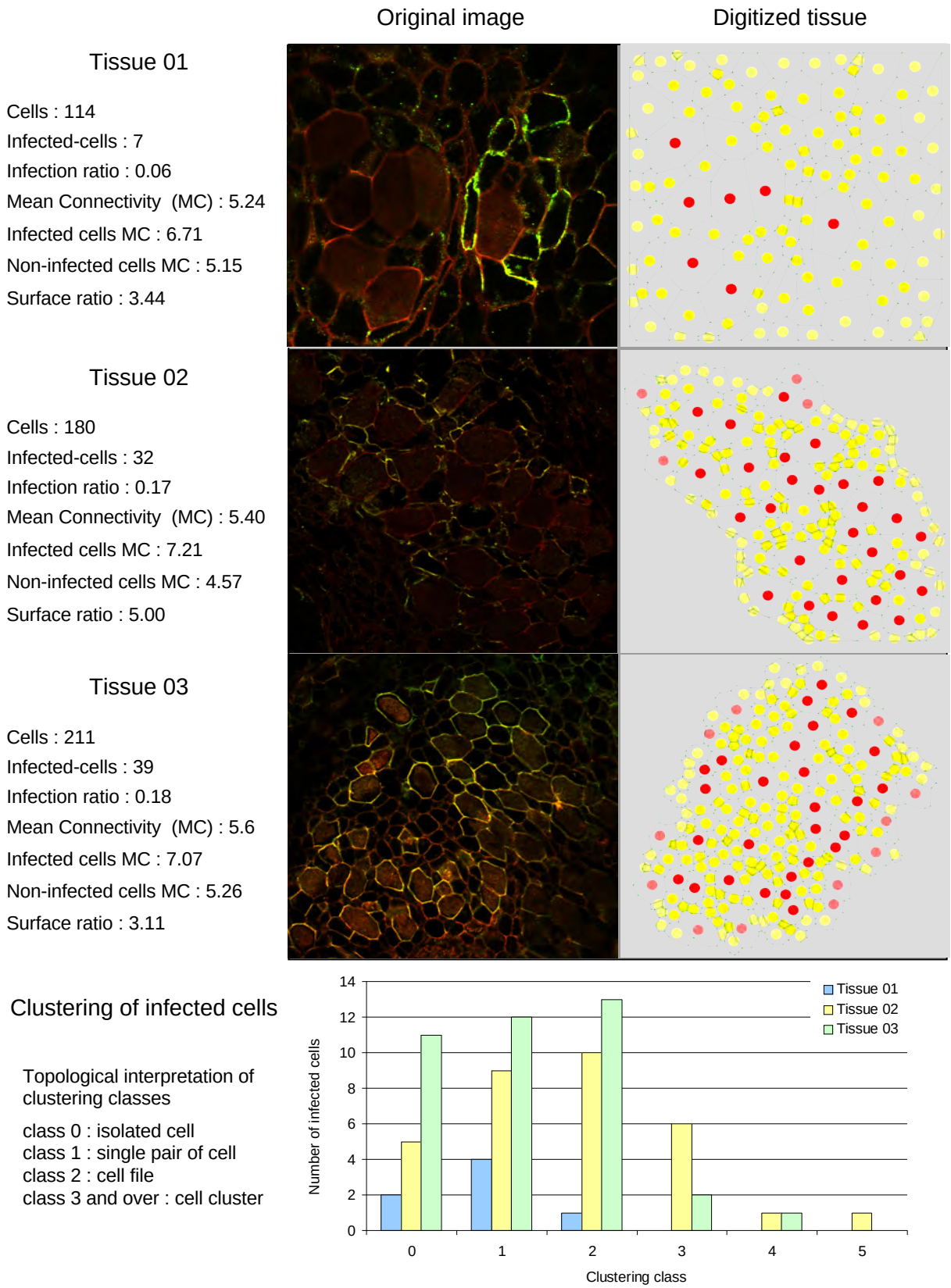

Fig. S2. Topology and digitization of symbiotic tissues. Three distinct nodule cortex tissues were manually digitized and modeled using the VisuAlea modeling platform. Infection ratio is the number of infected cells (red) over the number of non-infected cells (yellow). Mean connectivity is the mean number of cells neighboring a given cell (*i.e.* in direct contact with it). Surface ratio is the ratio between the mean surface of infected cells and non-infected cells. The variation of those values between the tissues depends on the cutting and is representative of the variety of infection, topology and geometry found along the nodule.

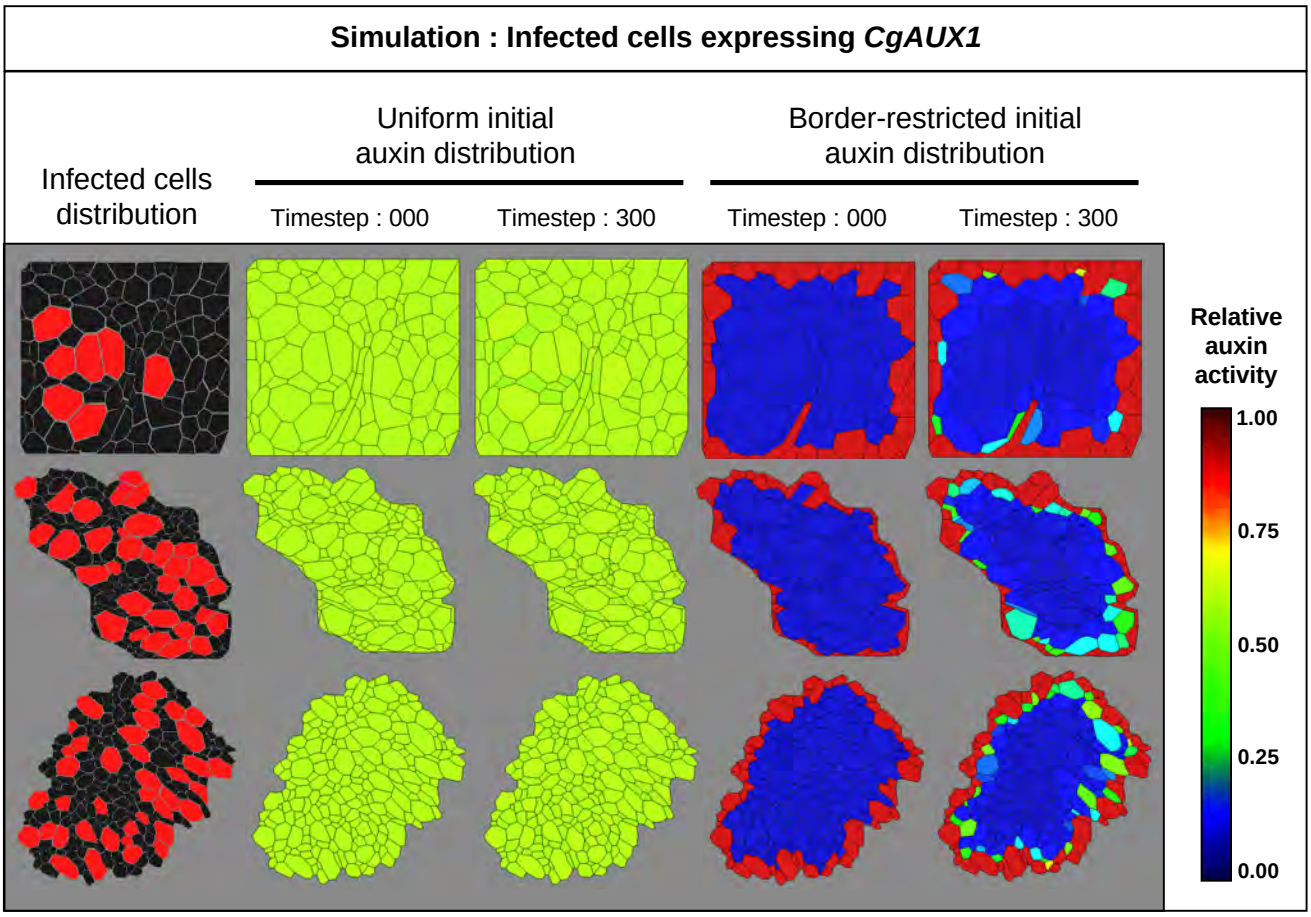

Fig. S3. Simulation of auxin distribution in virtual tissues with infected cells expressing *CgAUX1*. Two starting situations were considered for all three tissues. When auxin is initially uniformly distributed, a very slow accumulation takes place in the infected cells. When auxin comes from the border of the tissue, only the peripheral infected cells slowly accumulate auxin. The total amount of auxin is the same in both initial conditions, only the initial distribution varies. Auxin activity is the relative auxin concentration within the cells and its representation is capped at value 1. The equations that govern diffusive and active transport are discussed in detail in Text S1 (model notes).

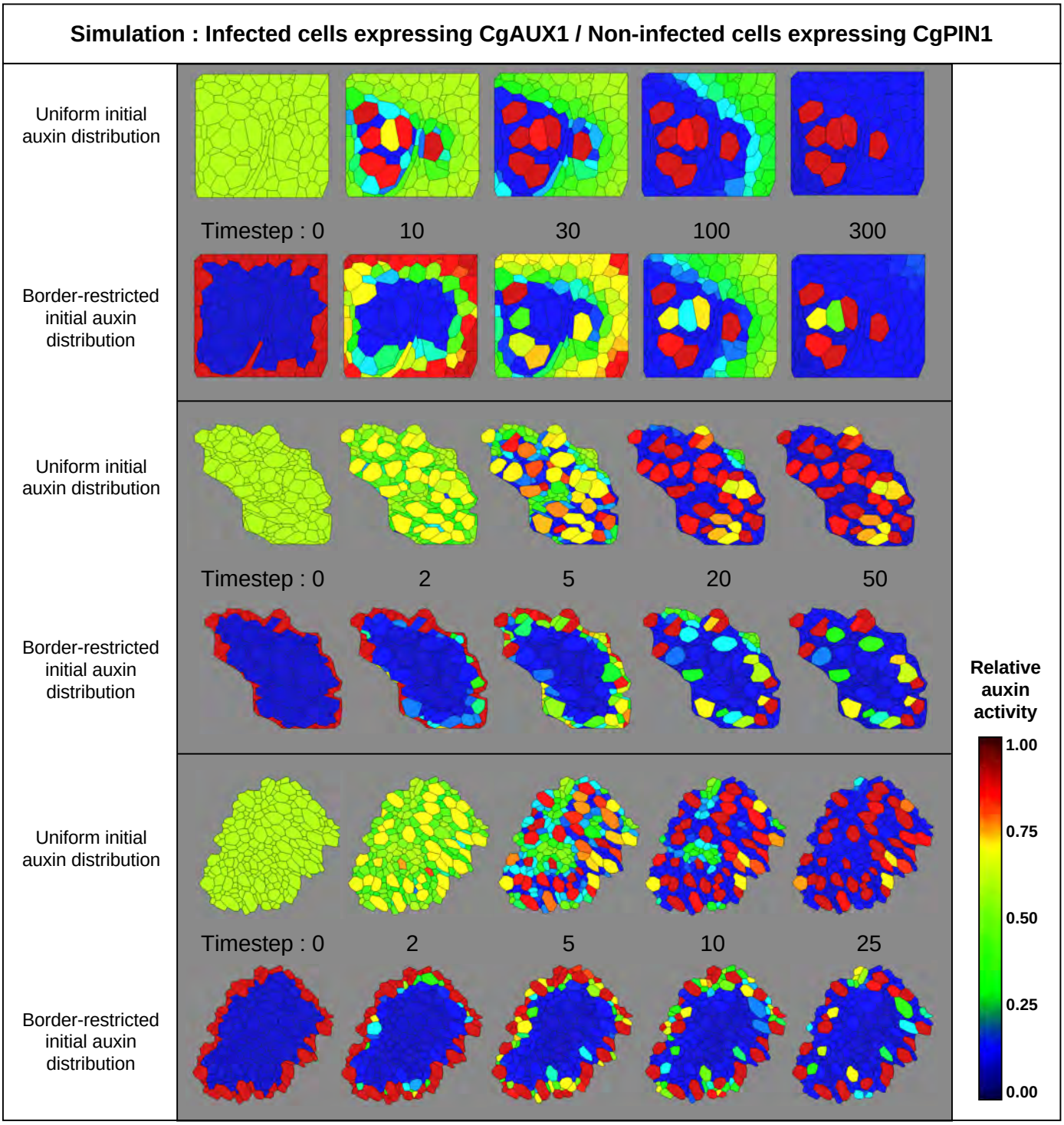

Fig. S4. Simulation of auxin distribution in virtual tissues with infected cells expressing *CgAUX1* and non-infected cells expressing *CgPIN1*. Two starting situations were considered for the three virtual tissues. When auxin is initially uniformly distributed, a rapid accumulation takes place in the infected cells and the surrounding non-infected cell are auxin depleted. When auxin comes from the border of the tissue, only the peripheral infected cells accumulate auxin even though the rest of the tissue is auxin-depleted. The total amount of auxin is the same in both initial conditions, only the initial distribution varies. Auxin activity is the relative auxin concentration within the cells and its representation is capped at value 1. The equations that govern diffusive and active transport are discussed in detail in Text S1 (model notes).

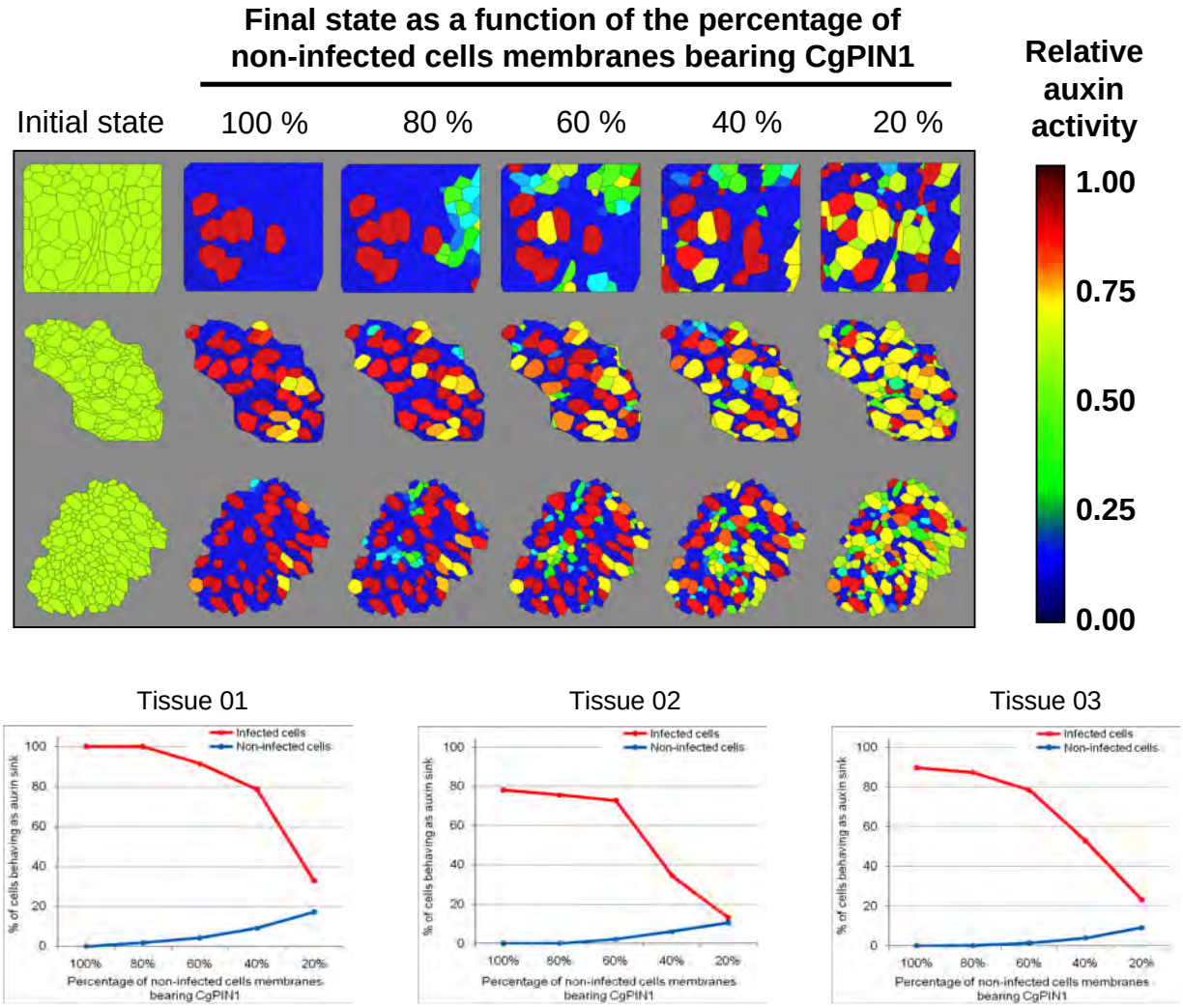

Fig. S5. Robustness of auxin distribution against CgPIN1 perturbation. We assessed whether the robustness of auxin distribution depended on the localization of CgPIN1 in all the non-infected cell membranes by simulating auxin distribution in tissue where a varying percentage of non-infected cell membranes were randomly devoid of CgPIN1. The upper panel illustrates typical final auxin distributions in the three virtual nodules according to the percentage of non-infected cell membranes bearing CgPIN1. The lower panel shows the percentage of infected and non-infected cells behaving as auxin sinks (i.e. accumulating over 0.9 unit of auxin during the course of the simulation) as a function of the percentage of non-infected cell membranes devoid of CgPIN1 (each data point correspond to 10 simulation runs). The number of infected cells behaving as auxin sinks only drops significantly when less than 60% of non-infected cell membranes are devoid of CgPIN1. The total amount of auxin in the virtual tissue is the same in all initial conditions for a given tissue, only the initial distribution varies. Auxin activity is the relative auxin concentration within the cells and its representation is capped at value 1. The equations that govern diffusive and active transport are discussed in detail in Text S1 (model notes).

Table S1: Genome data mining results. Functionally analyzed genes for indole acetic acid and phenyl acetic acid biosynthesis pathways were identified as described in Methods were used as query sequences. The best BlastP hits in the *Frankia* CcI3 genome are shown.

Pathway	Gene	Organism	Accession	*Frankia* CcI3 homolog(s)	e-value	% identity
IAA biosynthesis						
IAM	Tryptophan monooxygenase	*Agrobacterium tumefaciens*	AAD30489	No hit		
IAM	Indole-3-acetamide hydrolase	*Agrobacterium tumefaciens*	AAD30488	Francci3_3644	$1{,}00e^{-28}$	29
IPyA	Trypophan aminotransferase	*Azospirillum brasilense*	AAW50704	Francci3_4054	$6,\ 00e^{-39}$	30
IPyA	Indole-3-pyruvate decarboxylase	*Enterobacter cloacae*	P23234	Francci3_3640	$6,\ 00e^{-19}$	24
IPyA	Phenylpyruvate decarboxylase	*Azospirillum brasilense*	P51852	Francci3_3640	$2,\ 00e^{-28}$	27
				Francci3_2495	$1,\ 00e^{-11}$	24
IPyA/TAM	Indole-3-acetaldehyde dehydrogenase	*Ustilago maydis*	AAC49575	Francci3_2944	$7,\ 00e^{-93}$	40
				Francci3_3777	$4,\ 00e^{-82}$	36
TAM	Tryptophan decarboxylase	*Catharanthus roseus*	AAA33109	Francci3_2867	$2,\ 00e^{-17}$	24
TAM	Amine oxidase	*Klebsiella aerogenes*	P49250	No hit		
IAN	Arylacetonitrilase	*Alicaligenes faecalis*	BAA02684	Francci3_1242	$1,\ 00e^{-06}$	24
PAA Biosynthesis						
Phenyl pyruvate	Phenylalanine aminotransferase	*Lactococcus lactis*	AAF06954	Francci3_0566	$6,\ 00e^{-46}$	32
				Francci3_3813	$4,\ 00e^{-44}$	30
Phenyl pyruvate	Phenylpyruvate decarboxylase	*Azospirillum brasilense*	P51852	Francci3_3640	$2,\ 00e^{-28}$	27
				Francci3_2495	$1,\ 00e^{-11}$	24
Phenyl pyruvate	Phenylacetaldehyde dehydrogenase	*Pseudomonas putida*	ABR57228	Francci3_2944	$0,\ 00e^{+00}$	65
				Francci3_3777	$9,\ 00e^{-76}$	36

Table S2: Primers used for gene expression analyses.

Gene	Primer name	Sequence
CgAUX1	qCgAUX1F	5'-ACCAGGAGCAACCGGAAGAC-3'
	qCgAUX1R	5'-AGCACTTGCGCAACTTGATTG-3'
CgLAX3	qLAX3F	5'-GGAAACTGCGTGGAAATGGA-3'
	qLAX3R	5'-CACTTGCGCGACCTGGTTAG-3'
CgPIN1	CgPINlike-F	5'-AACTCGCCAACGCTCCAG-3'
	CgPINlike-R	5'-TTGACGCCATTCCTTGTTCC-3'
Francci3_0566	Francci3_0566F	5'-GTTCTACTGCTATCCGTCG-3'
	Francci3_0566R	5'-GCTGACTCCCTTGACGAG-3'
Francci3_4054	Francci3_4054F	5'-GCTACCTGGACTGCCTG-3'
	Francci3_4054R	5'-ACTTCACATCGCTCCC-3'
Francci3_3640	Francci3_3640F	5'-CGCATATGATCCACTGTTCG-3'
	Francci3_3640R	5'-GCACCGAGTCCATGTAGG-3'
Francci3_1249	Francci3_1249F	5'-GCCGCCCGTCACGAACTC-3'
	Francci3_1249R	5'-ACCAGGCTCACGAACGACAG-3'
Francci3_3777	Francci3_3777F	5'-GAACACCTCGGACTGGATG-3'
	Francci3_3777R	5'-GGGCGGGCTACTTCTACC-3'
Francci3_2944	Francci3_2944F	5'-GCGGCATTCGGCGGATAC-3'
	Francci3_2944R	5'-TGTTCTTGGTCTGGCTGTAGTG-3'
Francci3_2495	Francci3_2495F	5'-AAGCCAGCCACAAGATGGTGAT-3'
	Francci3_2495R	5'-AATCAACTGGCGCAGCGTCT-3'
RpsA	RpsAFrancci_1057F	5'-CGAAGTCCGTTCCGAGTTC-3'
(*Francci3_1057*)	RpsAFrancci3_1057R	5'-CGCCGAAGTTGACGATGG-3'
AtpD	AtpDFrancci3_3707F	5'-GGCAAGACCGTCATCATC-3'
(*Francci3_3707*)	AtpDFrancci3_3707R	5'-GTCATCTCCAGGAACAGG-3'

Model description for 'Auxin carriers localization drives auxin accumulation in plant cells infected by *Frankia* in *Casuarina glauca* actinorhizal nodules'

The model investigates the role of the PIN and AUX1 proteins by simulating auxin transport through the tissue. The results are produced using OpenAlea [1, 17], which is a vertex-based modelling framework that enables us to prescribe realistic cell geometries (drawn using confocal images) and simulate the auxin fluxes. We consider two-dimensional arrays of cells and the auxin concentration within each cell is governed by a deterministic ordinary differential equation that depends on the cell geometries, the auxin concentrations of neighbouring cells, the concentration of PIN and AUX1 proteins on the cell membranes, and the pH. Many researchers have successfully used modelling approaches to simulate auxin transport and gain understanding of the emergent auxin distributions (see [3, 12, 13] for reviews); the following description is based on that by Band *et al.* [2]

We describe first the equations governing the cell-to-cell auxin transport by considering the movement of auxin between two cells and the cell wall that lies between them. As shown in figure 1, we describe the auxin transport by considering three compartments, namely cell 1, cell 2, and cell wall. We assume that auxin transport within each compartment is sufficiently fast that the auxin concentration is spatially homogeneous, and we denote the auxin concentrations in the cell 1, cell 2 and cell-wall compartments by $a_1(t)$, $a_2(t)$ and $a_w(t)$ respectively. Cell 1 is separated from the cell wall by membrane 1 and similarly cell 2 by membrane 2. These membranes may contain PIN and AUX1 proteins. Considering membrane j (for $j = 1, 2$), we set $PIN_j = 1$ if the membrane contains PIN proteins and $PIN_j = 0$ if PIN proteins are not present; similarly, we set $AUX1_j = 1$ or $AUX_2 = 0$ to prescribe the presence or absence of AUX1 proteins respectively. We denote the area of cell 1 and cell 2 by V_1 and V_2, the area of the wall compartment by V_w and the length of the cell wall and adjacent cell membranes by S.

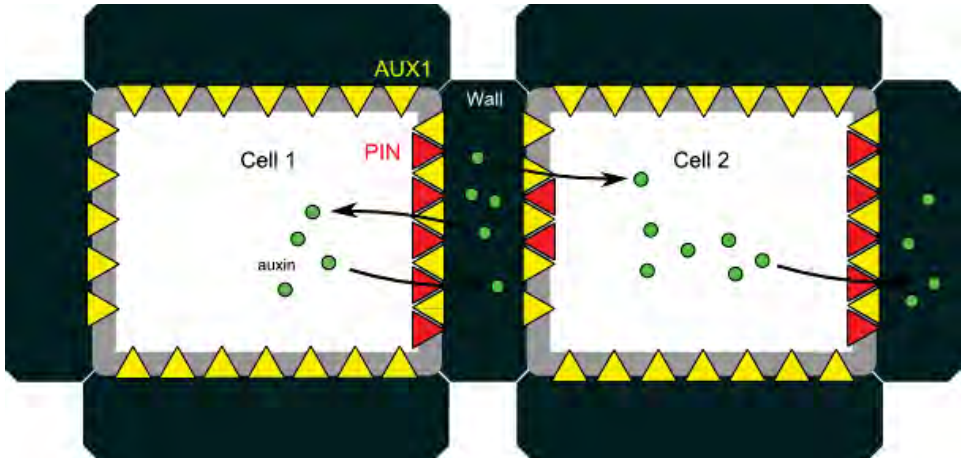

Figure 1: We describe the auxin fluxes between two adjacent cells and the intervening cell wall.

Within the tissue, auxin is present in both protonated and anionic forms; the proportion of each is determined by the pH of the region in which it is located and the dissociation constant, pK, such that the proportion of protonated auxin in the cell-wall and cell compartments are given by

$$A_1 = \frac{1}{1+10^{pH_w - pK}}, \quad B_1 = \frac{1}{1+10^{pH_c - pK}}, \tag{1}$$

respectively, where pH_c denotes the cell pH and pH_w the cell-wall pH. Thus, for example, in cell 1 the concentration of protonated auxin is $B_1 a_1$ and that of anionic auxin is $(1-B_1)a_1$. Auxin moves between the cell and the cell wall by crossing the plasma membrane. We separate the auxin fluxes through each membrane from the cell to the cell wall (*i.e.* the number of molecules passing through the membrane per unit membrane length) into distinct components, namely the passive diffusive flux, J_{IAAH}, the active influx facilitated by the AUX1 membrane proteins, J_{AUX1}, and the active efflux facilitated by the PIN membrane proteins, J_{PIN}. With no PIN or AUX1 proteins, the membrane is impermeable to anionic auxin [18], and so the passive diffusive flux, J_{IAAH}, is driven by the concentration difference in protonated auxin. Thus, considering membrane 1, for example, the passive flux per unit length from cell 1 into the cell wall is given by

$$J_{IAAH} = P_{IAAH}\Big(B_1 a_1 - A_1 a_w\Big), \tag{2}$$

where P_{IAAH} is the passive membrane permeability. In contrast, the influx and efflux carriers actively transport anionic auxin by exploiting the electrochemical gradient across the cell mem-

brane. As in [7, 15, 16, 18, 20], we model the carrier-mediated flux using Goldman-Hodgkin-Katz theory [10]. The carrier-mediated flux from the cell to the cell wall due to the efflux carriers, J_{PIN}, is therefore described by the Nerst-Planck equation:

$$J_{PIN} = -D_m\left(\frac{\partial c}{\partial x_m} + \frac{zF_D c}{RT}\frac{\partial \phi}{\partial x_m}\right), \tag{3}$$

where $c(x_m)$ is the auxin concentration within the membrane, x_m is the distance through the membrane (with $x_m = 0$ being at the boundary with the cell compartment), D_m is the coefficient of diffusion within the membrane (due to the carriers), ϕ is the potential within the membrane, $z = -1$ is the valence of the anionic auxin, F_D is Faraday's constant, R is the gas constant and T is the temperature (which we take to be constant). We note that the flux, (3), has two components: the first term on the right-hand side describes the passive diffusive component and the second term describes the flux component that is driven by the electrochemical gradient across the cell membrane (see [10] for further details). We assume that the electric field is uniform within the membrane, such that $\mathrm{d}\phi/\mathrm{d}x_m = -V_m/l_m$, where V_m is the potential difference across the membrane (cytoplasmic potential minus cell-wall potential) and l_m is the membrane thickness, and we suppose that the time scale of transport across the membrane is sufficiently fast that the flux, J_{PIN} can be treated as uniform within it. On solving (3) with $c(0) = (1 - B_1)a_1$ and $c(l_m) = (1 - A_1)a_w$, it follows that for membrane 1 the component of the active efflux per unit area from cell 1 into the cell wall is given by

$$J_{PIN} = P_{PIN}PIN_1\left(q(\tilde{\phi})(1 - B_1)a_1 - q(-\tilde{\phi})(1 - A_1)a_w\right), \tag{4}$$

where $P_{PIN}PIN_1 = D_m/l_m$ is the effective membrane permeability, $q(x) = x/(e^x - 1)$, and $\tilde{\phi} \equiv F_D V_m/RT$. The flux due to the AUX1 influx carriers is also modelled by the Goldman-Hodgkin-Katz equations; however, these carriers cotransport two protons with each anion of auxin [13, 14], a collection that has a positive valence, $z = 1$, and so, facilitated by the carriers, will travel down the potential gradient from the cell wall into the cell. Assuming that within the membrane the flux is constant and the electric field is uniform (as for the PIN proteins), the Nerst-Planck equation, (3), with $z = 1$ can be solved to provide a formula for the influx carriers contribution to the flux from cell 1 into the cell wall,

$$J_{AUX1} = -P_{AUX1}AUX1_1\left(q(\tilde{\phi})(1 - A_1)a_w - q(-\tilde{\phi})(1 - B_1)a_1\right), \tag{5}$$

where $P_{AUX1}AUX1_1$ is the effective permeability due to the influx carriers. To maintain concise notation, we define

$$A_2 = q(\tilde{\phi})(1 - A_1), \quad A_3 = q(-\tilde{\phi})(1 - A_1), \quad B_2 = q(-\tilde{\phi})(1 - B_1), \quad B_3 = q(\tilde{\phi})(1 - B_1). \tag{6}$$

We note that the passive components of the carrier-mediated active fluxes, (3), result in the influx carriers creating a small efflux, and the efflux carriers creating a small influx.

We can now formulate the total flux per unit length through the membranes as the sum of the three flux components, $J_{IAAH} + J_{PIN} + J_{AUX1}$, (2, 4, 5); thus, the fluxes from the cell wall into cell 1 and cell 2 are given by

$$\begin{aligned} J_{w1} = {} & (A_1 P_{IAAH} + A_2 P_{AUX1} AUX1_1 + A_3 P_{PIN} PIN_1) a_w \\ & -(B_1 P_{IAAH} + B_2 P_{AUX1} AUX1_1 + B_3 P_{PIN} PIN_1) a_1, \end{aligned} \tag{7a}$$

$$\begin{aligned} J_{w2} = {} & (A_1 P_{IAAH} + A_2 P_{AUX1} AUX1_2 + A_3 P_{PIN} PIN_2) a_w \\ & -(B_1 P_{IAAH} + B_2 P_{AUX1} AUX1_2 + B_3 P_{PIN} PIN_2) a_2, \end{aligned} \tag{7b}$$

respectively.

In addition to the cell and cell-wall compartments, we must also consider the '*Frankia* compartments' in the infected cells, and simulate auxin movement across the plasma membrane between the *Frankia* compartments and the cell cytoplasm (see figure 2). If cell i is infected, we denote the area of these *Frankia* compartments by V_{fi} and let the membrane separating them from the cytoplasm have length S_{fi}. The proportion of protonated auxin in the *Frankia* compartment depends on the pH of the *Frankia* compartment which we take to be identical to the pH of the cell wall; thus the proportion of protonated auxin is given by A_1. As for the cytoplasm-to-cell wall fluxes described above, protonated auxin passively diffuses between the cytoplasm and *Frankia* compartment, whereas anionic auxin requires membrane proteins to facilitate its transport. Thus, following (2) and (5), if we suppose that cell 1 is infected, the passive flux and AUX1-facilitated flux from the *Frankia* compartment into cell 1 are given respectively by

$$J_{IAAH} = P_{IAAH}\Big(A_1 a_f - B_1 a_1\Big), \quad J_{AUX1} = P_{AUX1} AUX1_1\Big(A_2 a_f - B_2 a_1\Big), \tag{8}$$

where a_f denotes the auxin concentration in the *Frankia* compartment. Hence, the total flux from the *Frankia* compartment into cell 1 is

$$J_{f1} = (A_1 P_{IAAH} + A_2 P_{AUX1} AUX1_1) a_f - (B_1 P_{IAAH} + B_2 P_{AUX1} AUX1_1) a_1. \tag{9}$$

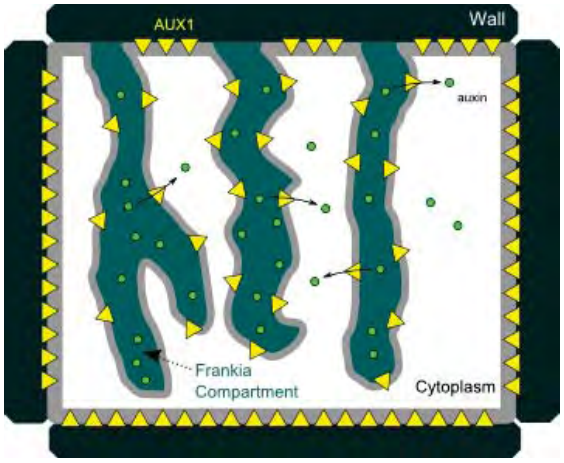

Figure 2: Diagram of an infected cell

In addition, the experimental data suggests that *Frankia* strains produce auxin, and therefore, we include a constant production rate in the *Frankia* compartments, denoted δ.
To derive the equations governing the auxin concentration within each compartment, we note that the rate of change of the number of auxin molecules in each compartment equals the sum of the various fluxes per unit membrane length into the compartment multiplied by the appropriate membrane length. Thus, considering only the fluxes between cell 1, cell 2, the *Frankia* compartment and the cell wall, the auxin concentrations can be described by

$$(V_1 - V_{f1})\frac{\mathrm{d}a_1}{\mathrm{d}t} = SJ_{w1} + S_f J_{f1}, \quad V_w \frac{\mathrm{d}a_w}{\mathrm{d}t} = -S(J_{w1} + J_{w2}), \tag{10a}$$

$$V_2 \frac{\mathrm{d}a_2}{\mathrm{d}t} = SJ_{w2}, \quad V_f \frac{\mathrm{d}a_f}{\mathrm{d}t} = \delta - S_f J_{f1}. \tag{10b}$$

Having derived the governing equations (10), we now simplify the model by exploiting the fact that the cell wall is thin, so that $0 < V_w/S \ll 1$. Thus, the concentration of auxin in the cell-wall compartment is approximately constant (see (10a)), and we can set $J_{w1} + J_{w2} \approx 0$. Using (7), this shows that the cell-wall concentration can be approximated by

$$a_w = \frac{\big((B_1 P_{IAAH} + B_2 P_{AUX1} AUX1_1 + B_3 P_{PIN} PIN_1)a_1 + (B_1 P_{IAAH} + B_2 P_{AUX1} AUX1_2 + B_3 P_{PIN} PIN_2)a_2\big)}{2A_1 P_{IAAH} + A_2 P_{AUX1}(AUX1_1 + AUX1_2) + A_3 P_{PIN}(PIN_1 + PIN_2)} \tag{11}$$

Thus, from (10), the auxin dynamics can be described by three coupled ordinary differential equations,

$$\begin{aligned}
\frac{\mathrm{d}a_1}{\mathrm{d}t} &= \frac{S}{(V_1 - V_{f1})}\big((A_1 P_{IAAH} + A_2 P_{AUX1} AUX1_1 + A_3 P_{PIN} PIN_1) a_w \\
&\qquad -(B_1 P_{IAAH} + B_2 P_{AUX1} AUX1_1 + B_3 P_{PIN} PIN_1) a_1\big) \\
&\quad + \frac{S_f}{(V_1 - V_{f1})}\big((A_1 P_{IAAH} + A_2 P_{AUX1} AUX1_1) a_f \\
&\qquad -(B_1 P_{IAAH} + B_2 P_{AUX1} AUX1_1) a_1\big), \qquad (12a) \\
\frac{\mathrm{d}a_2}{\mathrm{d}t} &= \frac{S}{V_2}\big((A_1 P_{IAAH} + A_2 P_{AUX1} AUX1_2 + A_3 P_{PIN} PIN_2) a_w \\
&\qquad -(B_1 P_{IAAH} + B_2 P_{AUX1} AUX1_2 + B_3 P_{PIN} PIN_2) a_2\big), \qquad (12b) \\
\frac{\mathrm{d}a_f}{\mathrm{d}t} &= \delta - \frac{S_f}{V_f}\big((A_1 P_{IAAH} + A_2 P_{AUX1} AUX1_1) a_f - (B_1 P_{IAAH} + B_2 P_{AUX1} AUX1_1) a_1\big), \qquad (12c)
\end{aligned}$$

where a_w is given by (11). Equivalent formula are used when we simulate the auxin dynamics between numerous cells, except then the flux into each cell will have contributions from each of the neighbouring cells. At the boundaries of the tissue, there is no auxin flux and therefore the total amount of auxin is conserved.

The biologically relevant parameter estimates used in the model simulations are summarised in Table 1. The cell-membrane permeabilities, P_{IAAH}, P_{AUX1}, and P_{PIN}, are key model parameters. Delbarre and coworkers [5, 6] measured the passive-diffusion membrane permeability in tobacco cells as $0.14 - 0.18\,\mathrm{cm\,hr^{-1}}$ and the majority of previous modelling studies use estimates around these values [4, 7, 8, 9, 11, 18]; thus following [8, 11, 18], we set $P_{IAAH} = 0.2\,\mathrm{cm\,hr^{-1}} = 0.56\,\mu\mathrm{m\,s^{-1}}$. Experimental values for the membrane permeabilities due to the influx and efflux carriers have not been well characterised. Delbarre [5] reports a carrier-mediated auxin influx and efflux in suspension-cultured tobacco cells, which has been used to estimate an influx carrier permeability of $0.02\,\mathrm{cm\,hr^{-1}}$ and an efflux carrier permeability of $0.01\,\mathrm{cm\,hr^{-1}}$ [18]. In addition, Szponarski *et al.* [19] measured an influx carrier permeability of $0.011\,\mathrm{cm\,hr^{-1}}$ in plasma-membrane vesicles derived from mature Arabidopsis leaves. However, these estimates were an average over all the cells therefore we would expect the actual values to be larger for the cell membranes containing AUX1 and PIN proteins. Previous models are in agreement about the permeability due to the influx carriers, and use $P_{AUX1} = 0.2\,\mathrm{cm\,hr^{-1}} = 0.56\,\mu\mathrm{m\,s^{-1}}$ [8, 11, 18]. In contrast, various values are used for the permeability due to the efflux carriers, including $0.124\,\mu\mathrm{m\,s^{-1}}$ [7, 9], $0.27\,\mu\mathrm{m\,s^{-1}}$ [8, 11], $1.4\,\mu\mathrm{m\,s^{-1}}$ [11]. We therefore present simulations for a typical value of $P_{PIN} = 0.27\,\mu\mathrm{m\,s^{-1}}$;

however, simulations with different values produce qualitatively identical results. The parameter values, pH_c, pH_w, pK and V_m are well characterised, and we use the representative values given in [18]. The cells' areas and cell-walls' lengths are obtained from the confocal images using the OpenAlea framework.

The movement of auxin between the *Frankia* compartment and cytoplasm depends on the pH in the *Frankia* compartment which is currently unknown. We present results with the *Frankia* compartment's pH being equal to that of the cell wall, although the precise value does not affect the behaviour of the system. Finally, we must estimate the area of the *Frankia* compartments and the length of the enclosing cell membrane. The *Frankia* compartment consists of a winding tube, with a radius of approximately $r_f = 0.5\,\mu$m, that entirely fills the cell cytoplasm. Thus, in two dimensions, we suppose that the *Frankia* compartment is an array of tightly packed circles such that in cell 1 with an area of $V_1\,\mu\text{m}^2$ there are $N_{f1} = V_1$ circles representing the *Frankia* compartment. Thus, in the infected cells, the *Frankia* compartment will have area $V_{f1} = N_{f1}\pi r_f^2$ and the enclosing membrane will have length $S_f = 2N_{f1}\pi r_f$.

The number of auxin molecules is the same in each of the simulations. In simulations where the auxin concentration is initially spatially homogeneous, we set the initial auxin concentration to be 0.5 in each cell. Therefore, in simulations where all the auxin is initially in the border cells, we set the initial border-cell concentrations to be $\sum_{i=1}^{N} 0.5V_i / \sum_{j=1}^{N_b} V_j$ (where N is the total number of cells and N_b is the number of border cells) and take the remaining initial concentrations to be zero. Similarly, in simulations where all the auxin is initially in the *Frankia* compartments, the *Frankia*-compartments initial concentrations are $\sum_{i=1}^{N} 0.5V_i / \sum_{k=1}^{N_{infect}} V_{fk}$ (where N_{infect} is the number of infected cells), and the initial concentrations in the cell cytoplasms and walls are zero. Using these parameter estimates (summarised in Table 1), we obtain the following constants that describe the movement of auxin between the cell wall and the cytoplasm.

$$A_1 = 0.24, \quad A_2 = 3.57 \quad A_3 = 0.034, \quad B_1 = 0.004, \quad B_2 = 0.045, \quad B_3 = 4.68. \tag{13}$$

As expected, in the basic cytoplasm there is little protonated auxin ($B_1 \ll 1$) therefore passive diffusion predominantly causes auxin to enter the cytoplasm from the cell wall and there is only a very small passive flux from the cell wall to the cytoplasm. However, even in the acidic cell wall, only 24% of the auxin is protonated and therefore the remaining 76% of auxin in the cell wall requires influx carriers to enter the cytoplasm. If influx carriers are present, they produce a flux into the cell that is over ten times the passive diffusion (consider A_2/A_1).

Parameter	Description	Value
P_{IAAH}	passive membrane permeability	$0.56\,\mu\mathrm{m\,s^{-1}}$
P_{AUX1}	membrane permeability due to AUX1 influx carriers	$0.56\,\mu\mathrm{m\,s^{-1}}$
P_{PIN}	membrane permeability due to PIN1 and PIN2 efflux carriers	$0.27\,\mu\mathrm{m\,s^{-1}}$
pH_c	pH in the cells' cytoplasms	7.2
pH_w	pH in the cell wall	5.3
pK	dissociation constant for auxin	4.8
V_m	cell membrane potential	$-0.120\,\mathrm{V}$
T	temperature	$300\,\mathrm{K}$

Table 1: Dimensional parameters estimates

References

[1] `http://openalea.gforge.inria.fr/wiki/doku.php?id=openalea`.

[2] L.R. Band, M.J. Bennett, and J.R. King. Multiscale modelling of auxin transport in the root elongation zone. *In Preparation*, 2010.

[3] T. Berleth, E. Scarpella, and P. Prusinkiewicz. Towards the systems biology of auxin-transport-mediated patterning. *Trends Plant Sci.*, 12:151–159, 2007.

[4] A. Chavarrıa-Krauser, W. Jager, and U. Schurr. Primary root growth: a biophysical model of auxin-related control. *Funct. Plant Biol.*, 32:849–862, 2005.

[5] A. Delbarre, P. Muller, V. Imhoff, and J. Guern. Comparison of mechanisms controlling uptake and accumulation of 2, 4-dichlorophenoxy acetic acid, naphthalene-1-acetic acid, and indole-3-acetic acid in suspension-cultured tobacco cells. *Planta*, 198:532–541, 1996.

[6] A. Delbarre, P. Muller, V. Imhoff, J.L. Morgat, and H. Barbier-Brygoo. Uptake, accumulation and metabolism of auxins in tobacco leaf protoplasts. *Planta*, 195:159–167, 1994.

[7] M.H.M. Goldsmith, T.H. Goldsmith, and M.H. Martin. Mathematical analysis of the chemosmotic polar diffusion of auxin through plant tissues. *P. Natl Acad. Sci. USA*, 78:976–980, 1981.

[8] M.G. Heisler and H. Jönsson. Modeling auxin transport and plant development. *J. Plant Growth Regul.*, 25:302–312, 2006.

[9] H. Jönsson, M.G. Heisler, B.E. Shapiro, E.M. Meyerowitz, and E. Mjolsness. An auxin-driven polarized transport model for phyllotaxis. *P. Natl Acad. Sci. USA*, 103:1633–1638, 2006.

[10] J. Keener and J. Sneyd. *Mathematical Physiology*. Springer, USA, 2004.

[11] E.M. Kramer. PIN and AUX/LAX proteins: their role in auxin accumulation. *Trends Plant Sci.*, 9:578–582, 2004.

[12] E.M. Kramer. Computer models of auxin transport: a review and commentary. *J. Exp. Bot.*, 2007.

[13] E.M. Kramer, X. Draye, and M.J. Bennett. *Practical systems biology*, chapter Modelling root growth and development. Taylor and Francis group, New York, USA, 2008.

[14] T. L. Lomax, R. J. Mehlhorn, and Briggs W. R. Active auxin uptake by zucchini membrane vesicles: quantitation using ESR volume and ΔpH determinations. *Proc. Natl Acad. Sci. USA*, 82:6541–6545, 1985.

[15] M.H. Martin, M.H.M. Goldsmith, and T.H. Goldsmith. On polar auxin transport in plant cells. *J. Math. Biol.*, 28:197–223, 1990.

[16] G.J. Mitchison. The dynamics of auxin transport. *P. Roy. Soc. Lond. B Bio.*, 209:489–511, 1980.

[17] C. Pradal, F. Boudon, C. Nouguier, J. Chopard, and C. Godin. Plantgl : a python-based geometric library for 3d plant modelling at different scales. *Graph. Models*, 71(1):1–21, 2009.

[18] R. Swarup, E.M. Kramer, P. Perry, K. Knox, H.M.O. Leyser, J. Haseloff, G.T.S. Beemster, R. Bhalerao, and M.J. Bennett. Root gravitropism requires lateral root cap and epidermal cells for transport and response to a mobile auxin signal. *Nat. Cell Biol.*, 7:1057–1065, 2005.

[19] W. Szponarski, O. Guibal, M. Espuna, P. Doumas, M. Rossignol, and R. Gibrat. Reconstitution of an electrogenic auxin transport activity mediated by Arabidopsis thaliana plasma membrane proteins. *FEBS lett.*, 446:153–156, 1999.

[20] J. Twycross, L.R. Band, M.J. Bennett, J.R. King, and N. Krasnogor. Stochastic and deterministic multiscale models for systems biology: an auxin-transport case study. *BMC Syst. Biol.*, 4:34, 2010.